Spatial analysis reveals combinative role for natural killer and CD8 T cells in antitumor immunity despite profound MHC class I loss in non-small cell lung cancer

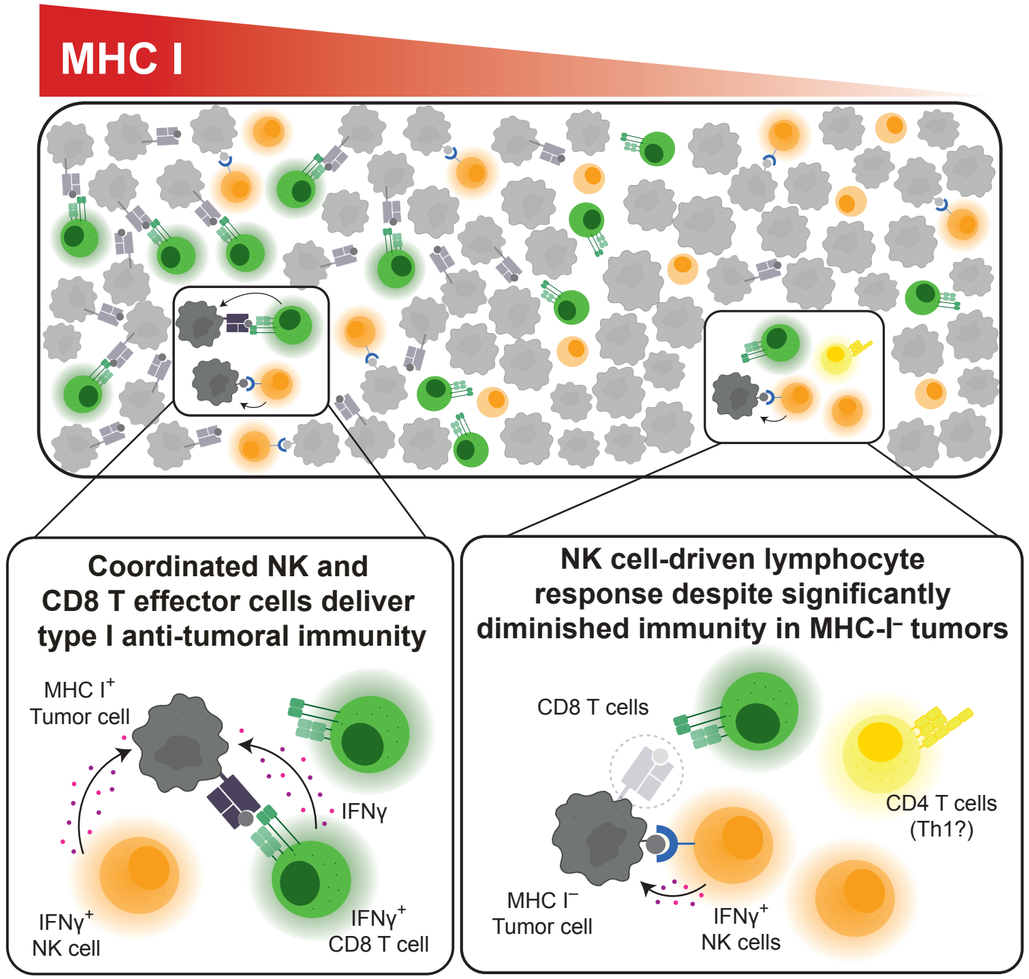

Authors

Remziye E. Wessel, Nardin Ageeb, Joseph M. Obeid, Ileana Mauldin, Kate A. Goundry, Mahdin Hossain, Ryan D. Gentzler, Nolan A. Wages, Craig L. Slingluff Jr, Timothy N.J. Bullock, Sepideh Dolatshahi†, and Michael G. Brown†

†Co-correspondence:

mgb4n@virginia.edu and sd8us@virginia.edu

In brief

Tumor-infiltrated natural killer (NK) and CD8 T cells display increased evidence of co-localization and coordinated effector activity in human MHC-I-bearing NSCLC tumors.

Spatial analysis reveals combinative role for natural killer and CD8 T cells in antitumor immunity despite profound MHC class I loss in non-small cell lung cancer

Running Title: NK and CD8 T cells antitumor immunity in NSCLC

Remziye E. Wessel,[1] Nardin Ageeb,[2] Joseph M. Obeid,[3] Ileana Mauldin,[4] Kate A. Goundry,[1] Mahdin Hossain,[5] Chad Lehman,[5] Ryan D. Gentzler,[6] Nolan A. Wages,[7] Craig L. Slingluff Jr,[4] Timothy N.J. Bullock,[5,8] Sepideh Dolatshahi,[1,5†] and Michael G. Brown [5,9-11†]

[1]Department of Biomedical Engineering, University of Virginia School of Medicine, Charlottesville, Virginia 22908

[2]Department of Biology, University of Virginia School of Medicine, Charlottesville, Virginia 22908

[3] Department of Thoracic Surgery, Temple University Hospital, Philadelphia, Pennsylvania 19140

[4]Department of Surgery, University of Virginia School of Medicine, Charlottesville, Virginia 22908

[5]Beirne B. Carter Center for Immunology Research, University of Virginia School of Medicine, Charlottesville, Virginia 22908

[6]Department of Medicine, Hematology and Oncology, University of Virginia School of Medicine, Charlottesville, Virginia 22908

[7]Department of Biostatistics, Virginia Commonwealth University, Richmond, Virginia 23298-0032

[8]Department of Pathology, University of Virginia School of Medicine, Charlottesville, Virginia 22908

[9]Department of Medicine, Nephrology, University of Virginia School of Medicine, Charlottesville, Virginia 22908

[10]Center for Immunity, Inflammation and Regenerative Medicine, University of Virginia School of Medicine, Charlottesville, Virginia 22908

[11]Department of Microbiology, Immunology and Cancer Biology, University of Virginia School of Medicine, Charlottesville, Virginia 22908

[†]Shared senior authorship.

Keywords: MHC class I, CD8 T cells, natural killer cells, tumor-infiltrating lymphocytes, interferon-gamma, multiplex immunofluorescence, patient survival, tissue micro-array, spatial analysis, systems immunology, intratumor heterogeneity, cell co-localization

Availability of data and material – Quantitative IHC and mIF data are available in a public, open-access repository (UVA Libra). Algorithms developed for this study (O-PLSDA and cell neighborhood scoring) are available on GitHub (https://github.com/Dolatshahi-Lab). IHC and mIF images will be made available by the authors upon reasonable request.

Competing interests – CLS - Research support to the University of Virginia from Celldex (funding, drug), Merck (funding, drug), Theraclion (device staff support); Funding to the University of Virginia from Polynoma for PI role on the MAVIS Clinical Trial; Funding to the University of Virginia for roles on Scientific Advisory Boards for Immatics and CureVac. CLS also receives licensing fee payments through the UVA Licensing and Ventures Group for patents for peptides used in cancer vaccines. RDG – Research support to the University of Virginia from Pfizer, Amgen, Chugai,

Merck, AstraZeneca, Janssen, Daiichi Sankyo, Alliance Foundation, Takeda, ECOG/ACRIN, Jounce Therapeutics, Bristol Myers Squibb, SWOG, Helsinn, Dizal Pharmaceuticals, and Mirati. RDG received payment for service on Scientific Advisory Boards including AstraZeneca, Takeda, Gilead, Janssen, Mirati, Daiichi Sankyo, Sanofi, Oncocyte, Jazz Pharmaceuticals, Blueprint Medicines, and Merus.

Funding – This work was funded by a Cancer Team Science Award from the University of Virginia Comprehensive Cancer Center (TNJB & MGB), and a Collaborative Research Award from the University of Virginia Beirne Carter Center for Immunology Research (TNJB, SD & MGB). The UVA Comprehensive Cancer Center Support Grant (P30CA044579) from the NCI additionally supported work performed by the Biorepository and Tissue Research Facility (BTRF) and Molecular Immunologic and Translational Science (MITS) cores. REW received training support from National Institute of General Medical Sciences of the National Institutes of Health (T32-GM145443). JMO received training support from National Cancer Institute T32 CA163177 and the University of Virginia Department of Surgery. MH received training support through the University of Virginia College Science Scholar Summer Research stipend. CL received training support through the University of Virginia School of Medicine Summer Medical Research Internship Program.

Authors contributions – REW, SD and MGB wrote the manuscript with input from all authors. REW, NA, JMO, IM, KAG, CL, RDG, CLS, TNJB, SD and MGB contributed to the conception, design, and development of the project. REW, NA, JMO, IM, KAG, MH, and NW performed experiments and/or analyzed data. All authors read and approved the final version of the manuscript.

Acknowledgements – This work has been presented at the 2023 American Association of Immunologists (AAI) Annual Meeting (Abstract 62.08). We thank the University of Virginia BTRF and MITS cores at UVA for outstanding technical support. We thank Gabriel Hanson for helpful discussion.

Authors' information (optional) –

Michael G. Brown – ORCID iD 0000-0003-2872-7685

Timothy N.J. Bullock – ORCID iD 0000-0001-6141-3261

Sepideh Dolatshahi – ORCID iD 0000-0003-0226-0933

Ryan D. Gentzler – ORCID iD 0000-0002-8983-6677

Joseph Obeid – ORCID iD 0000-0002-6111-9289

Craig L. Slingluff – ORCID ID 0000-0002-6664-4373

Remziye E. Wessel – ORCID iD 0000-0002-8596-4700

List of abbreviations – Non-small cell lung cancer, NSCLC; squamous cell carcinoma, SCC; MHC class I, MHC-I; natural killer cell, NK cell; multiplexed immunofluorescence, mIF; interferon gamma, IFNγ; checkpoint inhibitor immunotherapy, CPI; orthogonalized partial least squares discriminant analysis, OPLSDA; variable importance in projection, VIP.

88 **ABSTRACT**

89 **Background.** MHC class I (MHC-I) loss is frequent in NSCLC and renders tumor cells resistant
90 to T cell lysis. NK cells kill MHC-I deficient tumor cells, and although previous studies indicate
91 their presence in NSCLC tumor margins, they were also functionally impaired. The goal of this
92 study was to evaluate whether NK cell and CD8 T cell infiltration and activation vary with MHC-I
93 expression. **Methods**. We used single-stain immunohistochemistry (IHC) and Kaplan-Meier anal-
94 ysis to test the effect of NK cell and CD8 T cell infiltration on overall and disease-free survival. To
95 delineate immune covariates of MHC-I-disparate lung cancers, we used multiplexed immunoflu-
96 orescence (mIF) imaging followed by multivariate statistical modeling. To identify differences in
97 infiltration and intercellular communication between IFNγ-activated and non-activated lympho-
98 cytes, we developed a computational pipeline to enumerate single cell neighborhoods from mIF
99 images followed by multivariate discriminant analysis. **Results**. Spatial quantitation of tumor cell
100 MHC-I expression revealed intra- and inter-tumoral heterogeneity, which was associated with the
101 local lymphocyte landscape. IHC analysis revealed that high numbers of $CD56^+$ cells in patient
102 tumors were associated with disease-free and overall survival ($p<0.05$). The overall survival as-
103 sociation strengthened considerably with high counts of both $CD56^+$ and $CD8^+$ cells ($p<1x10^{-4}$).
104 mIF imaging and multivariate discriminant analysis revealed an enrichment of both $CD3^+CD8^+$ T
105 cells and $CD3^-CD56^+$ NK cells in MHC-I-bearing tumors ($p<0.05$). To infer associations of func-
106 tional cell states and local cell-cell communication, we analyzed spatial single cell neighborhood
107 profiles to delineate the cellular environments of $IFNγ^{+/-}$ NK cells and T cells. We discovered that
108 both $IFNγ^+$ NK and CD8 T cells were more frequently associated with other $IFNγ^+$ lymphocytes in
109 comparison to $IFNγ^-$ NK cells and CD8 T cells ($p<1x10^{-30}$). Moreover, $IFNγ^+$ lymphocytes were
110 most often found clustered near $MHC\text{-}I^+$ tumor cells. **Conclusions**. We demonstrate that tumor-
111 infiltrating NK cells and CD8 T cells jointly affect vital control of NSCLC tumor progression. Robust
112 association of NK and CD8 T cells was most evident in MHC-I-bearing tumors, especially in the

113 presence of IFNγ. Frequent co-localization of IFNγ$^+$ NK cells with other IFNγ$^+$ lymphocytes in
114 near-neighbor analysis indicates lymphocyte activation is coordinately regulated in NSCLC.
115
116 **What is already known on this topic –** MHC-I loss occurs frequently in human NSCLC and
117 corresponds with a waning immune response in the tumor microenvironment (TME). NK cells
118 recognize "missing-self" targets and thus may be leveraged to target NSCLC tumors with sub-
119 stantial class I loss. While NK cell presence at tumor margins has been documented in the NSCLC
120 TME, they have been shown to lose function in this environment.
121
122 **What this study adds –** We developed spatial statistical analysis pipelines that leverage the local
123 heterogeneity of the tumor microenvironment at single cell resolution to rigorously test whether
124 NK cells and T cells together contribute antitumoral immunity in human lung cancer. We discov-
125 ered that a high density of tumor-infiltrating NK cells corresponded with disease-free survival, and
126 this association was considerably increased in patients with high coincident T cells, especially
127 those in central tumor. Intriguingly, both cell types were further found clustered together in MHC-
128 I-bearing tumors, especially when both were also expressing IFNγ, thus suggesting coordinated
129 lymphocyte activities may give rise to enhanced immune control of human lung cancer.
130
131 **How this study might affect research, practice, or policy –** This study provides a rationale for
132 developing novel immunotherapies that simultaneously increase NK and T cell anti-tumoral im-
133 munity. Robust associations linking NK cells with survival and IFNγ activity in NSCLC, including
134 in tumors with profound MHC-I loss, provides a basis for further research to evaluate the effect of
135 NK cells in MHC-I-deficient, CD8 T cell refractory NSCLC tumors.
136
137

138 **BACKGROUND**

139 Lung cancer is the leading cause of cancer-related death in the United States and globally, and
140 non-small cell lung cancer (NSCLC) accounts for approximately 85% of all lung cancers (1, 2).
141 Adenocarcinoma (AdenoCA) and squamous cell carcinoma (SCC) together account for the ma-
142 jority (~90%) of all NSCLC subtypes (3, 4). Both tumor types are infiltrated by diverse immune
143 cell types, including T cells and NK cells with cytokine and cytotoxic effector activity (5), highlight-
144 ing the opportunity to harness these cytolytic cells to mediate more efficacious control of human
145 lung cancer.

146 Tumor cell MHC class I (MHC-I) loss to evade recognition by cytotoxic T cells is common
147 in NSCLC, occurring in over 30% of human lung cancer cells and with over 90% having defects
148 of one or more MHC-I antigens and other molecules associated with antigen presentation (23).
149 This constitutes a logical evolutionary step given the propensity of NSCLC to have a large reper-
150 toire of antigenic mutations that can be presented to T cells on MHC-I (24). Despite the frequency
151 of MHC-I loss, its impact on lymphocyte infiltration and patient survival has not been resolved (25-
152 31).

153 The density of CD8 T cells infiltrating NSCLC tumors generally has been associated with
154 a favorable prognosis (6-8). However, assessment of patient risk based on this determination
155 alone is challenging due to factors such as the heterogeneity of intratumoral CD8 T cell infiltrates,
156 the inherent difficulty in reliably sampling and assessing tumor-infiltrating lymphocytes, a plausible
157 role for other immune cells, and because T cell exhaustion can contribute to poor immunological
158 control of lung cancers (9-11), thus implicating additional risk determinants. On the other hand,
159 NK cells have been shown to provide protection against hematological malignancies or metasta-
160 ses from primary tumors, yet their antitumor activity has been less evident in solid tumors (12,
161 13). Given their ability to recognize and lyse ‘missing-self’ targets, NK cells represent a presently

unharnessed, yet logical candidate to improve anti-tumor immunity in MHC-I deficient, CD8 T cell refractory lung tumors (32).

Prior work has shown that NK cells are prevalent in β2-microglobulin (β2m-)deficient NSCLC tumors (30), but intratumoral NK cells from NSCLC patients were found to have reduced IFNγ production and cytolytic capability compared to circulating NK cells from the same patients (33). Nonetheless, tumor-infiltrating NK cells activated by cytokines or stimulated via direct recognition of tumor cell expressed ligands of NK activating receptors have been shown to enhance tumor-specific T cells and control of tumor progression , possibly via cytokines to enhance recruitment or activation of classical dendritic cells (cDC. Understanding NK cell and CD8 T cell interactions that support the anti-tumor immune response in relation to MHC-I expression in the NSCLC tumor microenvironment (TME) is thus a priority.

Hypothesizing that NK cells and CD8 T cells might together drive anti-tumor immunity in NSCLC in relation to the level of tumor cell MHC-I expression, we investigated whether tumor-infiltrating NK cells and CD8 T cells were associated with patient survival, and if tumor cell MHC-I expression corresponded with variations in lymphocyte presence, activation status, or near-neighbor groupings in the NSCLC TME. Our findings suggest that novel strategies designed to target and leverage both T cells and NK cells in combined immune therapy may provide enhanced antitumor immunity and increased T cell activation, even in CD8 T cell refractory tumors.

MATERIALS AND METHODS

Immunohistochemistry. The AJCC 7th edition was used for clinical and pathological staging. An experienced pathologist outlined tumor areas and tumor margins. To identify regions of interest for further analysis, Hematoxylin-eosin staining was performed on sections from formalin-fixed,

186 paraffin embedded (FFPE) tissues. Central tumor (CT) and peripheral tumor (PT) 1 mm cores
187 were then extracted from the FFPE tissues based on the pathologist's annotation and used to
188 construct tissue microarray (TMA) samples from each of the 151 tumors as described (34).TMA
189 tissue sections were deparaffinized and rehydrated (34). Heat-induced antigen retrieval was per-
190 formed in citrate buffer for most antibodies (Abs), or in EDTA/high pH buffer for Abs to PH:10 as
191 described (34). NSCLC tissues were incubated with primary Abs to β2-microglobulin (mAb NAMB-
192 1, kindly provided by Soldano Ferrone), CD3 (mAb DAKO, clone 7.2.38), CD8 (clone C8/144B,
193 DAKO Carpinteria, CA), CD56 (mAb NCL-L-CD56-1B6, Leica), Granzyme B (Abcam ab4059),
194 and HLA class I heavy chains (HC) (HC10 (35), Ferrone lab). Enzyme-linked secondary antibod-
195 ies and 3,3'-diaminobenzidine (Dako) were used to develop the staining. Ab-stained slides were
196 counterstained with hematoxylin (Dako) and permanently mounted as described (34). Images
197 were acquired using a Nikon Digital Sight DS-Fi1 camera (Nikon Corporation, Tokyo, Japan), an
198 Eclipse 400 microscope (Nikon), or a NIS-Elements Viewer version 3.2 (Nikon). Staining control
199 tissues included tonsil, lymph node, and placenta. Tissues incubated with phosphate buffered
200 saline (PBS) instead of primary Ab and then stained with secondary Abs only served as negative
201 staining controls.

202

203 **TMA Immunotyping.** Tumor cell antigen expression (e.g., HLA class I) was assessed by a
204 pathologist and scored by their expression intensity (0 = no staining, 1 = mild staining, 2 = strong
205 staining) in each core. Scores from two cores per patient were summed to a total score that ranges
206 from zero to four in each tumor to account for tumor heterogeneity. Automated CD8 counting was
207 performed using a Leica SCN400 Scanner (Leica, Nussloch, Germany) and Digital Imaging Hub
208 (Leica) and validated by manual counting by a pathologist. Immune cell counts were reported as
209 counts per millimeter squared (mm^2).

210

211 **mIF imaging and geospatial analysis**. Five (5) µm-thick sections were cut from FFPE NSCLC
212 patient tissues from Cohort 2 (**table 2**). Human lymph node samples were used as a positive
213 control. mIF was performed according to the manufacturer's protocol using the OPAL Multiplex
214 Manual IHC kit and antigen retrieval (AR) buffers AR6 and AR9 (Akoya Biosciences, Marlborough,
215 Massachusetts, USA) and DIVA Decloaker AR buffer (Biocare Medical, Pacheco, California,
216 USA). Staining sequence, antibodies and AR buffers used are as follow: AR9, CD3 (1:100, Cell
217 Marque MRQ-39) Opal520; AR9, CD8 (1:500, clone C8/144B Agilent Technologies, Santa Clara,
218 California, USA) Opal540; AR6, CD56 (1:1000, CD56 (Cell Marque MRQ-42) Opal570; DIVA,
219 IFNγ (1:1000 NeoBiotechnologies 345 MSM4 P2 IFNG/466) Opal620; AR6, MHCI (1:15,000 HLA
220 class I heavy chains (HC10,(35) kindly provided by Soldano Ferrone) Opal650; AR6 Pancyt-
221 okeratin (1:200 MA513203, Invitrogen) Opal690, and AR6, spectral DAPI (Akoya Biosciences,
222 Marlborough, Massachusetts, USA) as described previously (36).

223 Stained slides were mounted using prolong diamond antifade (Life Technologies, Carls-
224 bad, California, USA) and scanned using the PerkinElmer Vectra 3.0 system and Vectra software
225 (Akoya Biosciences, Marlborough, Massachusetts, USA). Regions (3 mm^2) were identified using
226 Phenochart software and tissue images were acquired at 20x magnification with the Vectra 3.0
227 system. The images were spectrally unmixed using single stain positive control images in the
228 InForm software (Akoya Biosciences, Marlborough, Massachusetts, USA). A tissue classifier was
229 trained on $panCK^+$ tumor cells and $panCK^-$ stroma using HALO software (Indica Labs, Albuquer-
230 que, New Mexico, USA). Immune cells were enumerated using HALO software (Highplex FL
231 module). Lymphocyte density was quantified as density of cells expressing a given marker
232 (cells/mm^2) within stromal or tumor compartments of each region.

233 To increase statistical power while avoiding size-related representational biases in re-
234 sected patient tissues, a patient-agnostic, tissue regional analysis was developed to analyze
235 scanned images of lung adenocarcinoma and SCC patient tumor biopsies as independent entities

236 (**supplemental figure S1**). In total, 394 regions across 29 adenocarcinoma tumors and 108 re-
237 gions across 7 SCC tumors were collected. Regions with evident tumor cell CD56 expression or
238 fewer than 50 cells enumerated were excluded. The remaining 361 adenocarcinoma regions and
239 89 SCC regions were analyzed. To validate that over-representation of tumors with a greater
240 number of images did not bias our results, we iteratively sampled a random subset of images with
241 equal representation from all tumors and observed similar results.

242

243 **Correlation analyses**. Spearman correlation analyses of Cohort 1 and Cohort 2 were performed
244 in R statistical computing software (version 4.1.2) using the "corr" package. Visualizations were
245 generated using "ggplot2" and "corrplot" packages. Slides or regions with missing data were omit-
246 ted only from analyses requiring the use of those missing variables.

247

248 **Survival analyses**. Univariate and multivariate survival analysis was performed using R software
249 version 4.2.1. *Kaplan-Meier analysis*. To test the effect of NK cell and CD8 T cell abundances on
250 survival, tumors from patients in Cohort 1 were stratified at the median normalized cell counts
251 (cells/mm^2) averaged between CT and PT regions (CT NK cells + PT NK cells) / 2). The effect of
252 MHC-I expression on overall survival (OS, the time from resection to death by any cause) and
253 disease-free survival (DFS, the time from surgical resection to disease recurrence or death by
254 any cause) was determined by comparing patients with percent MHC-I expression above and
255 below the median value averaged between CT and PT. Significance was determined by a log-
256 rank test ($p < 0.05$). Tumors with missing data for any of these markers were excluded from those
257 respective analyses. *Cox proportional hazards modeling*. Proportional hazards assumptions were
258 tested using Schoenfeld residual analysis for univariate and multivariate analysis using a signifi-
259 cance level of 0.01. Multivariate Cox proportional hazards models assessed the relationship be-
260 tween survival endpoints (OS and DFS) and NK cell, CD8 T cell abundances, and MHC-I

261 expression, after adjusting for age and sex. Associations were considered significant for two-
262 sided *p* values ≤ 0.05.
263
264 **Cellular neighborhood analysis**. *Custom cell-cell neighborhood scoring algorithm*. Intercellular
265 geospatial colocalizations in NSCLC tumors from Cohort 2 were determined in Python using sin-
266 gle cell 2-dimensional coordinates obtained from HALO. The Euclidian distance between each
267 cell and every other cell on the slide was computed; nearest neighbors were defined as cells with
268 a center-to-center Euclidian distance of less than 30 μm from the center cell (**supplemental fig-
269 ure S2**). The nearest neighbors of each phenotype were enumerated to yield the neighborhood
270 profile for every individual cell. *Intercellular K function analyses.* Intercellular geospatial colocali-
271 zations in NSCLC tumors from Cohort 2 were further analyzed using the Spatstat package in R
272 version 4.2.1 (37). The K function was used to determine the number of nearest neighbors for a
273 given cell type as a function of radius up to 200 μm for each tumor region separately.
274
275 **Multivariate discriminant analyses**. Orthogonalized Partial Least Squares Discriminant Anal-
276 yses (OPLSDA) two-component (latent variable) models were generated in MATLAB (Release
277 R2022a, MathWorks, Natick, MA) using scripts developed in-house.
278 All data input to OPLSDA were log-transformed, centered, and scaled. First, OPLSDA
279 models were constructed on cell densities per region (cells/mm^2) to discriminate between tumor
280 regions from Cohort 2 with panCK+MHC-I+ cell counts above or below the median for AdenoCA
281 and SCC tumors separately. Cells localized to the tumor nest were normalized to tumor classified
282 area as determined by HALO software, and likewise for stromal cells. Second, OPLSDA models
283 were constructed to discriminate the cellular neighborhood profiles between activated and inacti-
284 vated NK cells (CD3$^-$ CD56$^+$ IFNγ±) and CD8 T cells (CD3$^+$ CD8$^+$ IFNγ±). Prediction accuracy
285 was determined using a random 5-fold cross validation framework. Significance was determined

286 empirically by comparing the constructed model's mean squared error against one thousand ran-
287 domly permuted null models (38, 39). Univariate comparisons between model features were con-
288 ducted using a non-parametric Wilcoxon rank sum test with a Benjamini-Hochberg false discovery
289 rate correction controlled at $p < 0.05$.
290

291 **RESULTS**

292 **Patient characteristics**. Specimens used to construct the TMA were collected from patients who
293 were treated at the University of Virginia between 2011 and 2014 and were analyzed by single-
294 stain immunohistochemistry (IHC) along with retrospective review of clinical records (IRB-HSR#:
295 18346) (Cohort 1, n = 151) (**table 1**). Whole tumor resections were collected prospectively from
296 patients treated at the University of Virginia between 2014 and 2018 and were analyzed by mul-
297 tiplexed immunofluorescence (mIF) (Cohort 2, n = 36). Two patients in Cohort 2 were treated with
298 Pembrolizumab, one was treated with Atezolizumab, and one was treated with Nivolumab. No
299 patients in Cohort 1 received immunotherapy.
300

301 **Table 1. NSCLC patient characteristics.**

		Cohort 1 (n = 151) (Retrospective)			**Cohort 2 (n = 36) (Prospective)**			
Clinical feature *		**AdenoCA** (n=93)	**SCCa** (n=58)	**Total Cohort 1**	**AdenoCA** (n=28)	**SCCa** (n=8)	**Total Cohort 2**	**Total (Cohort 1 + Cohort 2)**
Biologic sex	Female	49 (53%)	21 (36%)	70 (46%)	20 (71%)	5 (63%)	25 (69%)	95 (51%)
Age in years, mean +/- (range)		67 ± 9 (49-89)	66 ± 9 (38-84)	67 ± 9 (38-89)	66 ± 11 (47-85)	62 ± 12 (55-81)	65 ± 11 (47-85)	66 ± 9 (38-89)
AJCC v7 Stage at excision	Stage I	57 (61%)	36 (62%)	93 (62%)	7 (25%)	0 (0%)	7 (19%)	100 (53%)
	Stage II	20 (22%)	13 (22%)	33 (22%)	10 (36%)	2 (25%)	12 (33%)	45 (24%)
	Stage III	13 (14%)	8 (14%)	21 (14%)	11 (39%)	5 (63%)	16 (44%)	37 (20%)
	Stage IV	3 (3%)	1 (2%)	4 (3%)	0 (0%)	1 (13%)	1 (3%)	5 (3%)
Largest Tumor Diameter* in cm, Mean +/- SD (range)		2.7 ± 1.8 (0.6-12)	3.7 ± 2.4 (0.9-10)	3.1 ± 2.1 (0.6-12)	3.29 ± 1.58 (1.3-6.3)	3.03 ± 1.58 (1.2-5.5)	3.23 ± 1.56 (1.2-6.3)	3.12 ± 1.99 (0.6-12)
Prior chemotherapy		5 (6%)	1 (2%)	6 (4%)	6 (21%)	3 (38%)	9 (25%)	15 (8%)
Treated with Immunotherapy		0 (0%)	0 (0%)	0 (0%)	4 (14%)	0 (0%)	4 (11%)	4 (2%)
* number (%) unless otherwise specified								

302

303 **Broad MHC class I expression variation in human NSCLC is associated with variation in**
304 **intra-tumoral lymphocytes.** To examine the MHC-I expression in NSCLC tumors and its rela-
305 tionship with occupation by $CD56^+$ NK cells and CD8 T cells, we performed IHC on Cohort 1
306 (**table 1**) staining for anti-MHC-I heavy chain (HC), β2-microglobulin (β2m), CD56, and CD8. Cell
307 counts were enumerated in CT and PT cores (**Methods**). We observed wide-ranging MHC-I HC
308 expression levels in both AdenoCA and SCC, with greater than 90% MHC-I HC loss in 12% of
309 AdenoCA and 22% of SCC tumors (**figure 1A,B**). At the other extreme, 16 AdenoCAs (17%) and
310 10 SCCs (17%) had MHC-I expression in 100% of cells. We additionally observed heterogeneity
311 in tumor cell MHC-I HC expression within the tumors, as CT and PT cores of the same tumor
312 often displayed distinct MHC-I HC expression patterns (**figure 1A,B light bars vs dark bars**).
313 HC10 reacts with unfolded HLA-A, -B and -C heavy chains (33), so it may not identify HLA Class
314 I molecules folded with β2m; thus, we analyzed the correlation of β2m with HLA I HC expression.
315 HLA HC and β2m staining significantly correlated in both CT and PT regions in adenocarcinoma
316 and SCC (**figure 1C,E**), thus suggesting that loss of HC10 staining was primarily due to de-
317 creased surface expression of folded MHC-I dimers. Nonetheless, broad variability in MHC-I HC
318 for each β2m classification suggested other regulators of MHC-I expression and/or antigen
319 presentation may have affected MHC-I loss in Cohort 1. MHC-I loss thus is heterogeneously man-
320 ifest across NSCLC patient tumors comprising both AdenoCA and SCC, and these may develop
321 or progress differently in defined TME regions within individual patients.

322 Given its significant loss in NSCLC, we asked whether tumor cell MHC-I expression may
323 be associated with NK cell and CD8 T cell infiltrates into the TME. In pairwise Spearman correla-
324 tions of Cohort 1 TMA features, we found that the density of $CD56^+$ and $CD8^+$ cells significantly
325 correlated with expression levels of both MHC-I and β2m in both types of NSCLC (**figure 1D,F**).
326 Moreover, intra-tumoral $CD56^+$ cells correlated with $CD8^+$ cells, most profoundly in PT regions,
327 suggesting both cell types may interact and play a role in NSCLC tumor control.

328

329 **Concurrent tumor-infiltrating CD8$^+$ and CD56$^+$ immune cells are associated with patient**
330 **survival in human NSCLC independent of MHC-I expression.** Prior work has shown that the
331 density of tumor-infiltrating CD8 T cells is generally associated with better patient survival (6, 7).
332 Given the effect of tumor cell MHC-I expression on CD8 T cell and NK cell recognition, we asked
333 if MHC-I expression was associated with patient outcome. We did not detect any significant as-
334 sociation between and DFS or OS and MHC-I expressed above or below the median in CT, PT,
335 or averaged across CT and PT (**figure 2A,B, supplemental figure S3**). We thus investigated
336 whether densities of intra-tumoral CD8$^+$ or CD56$^+$ cells were associated with DFS or OS outcomes
337 for Cohort 1 patients (**figure 2C-F**). Intriguingly, high intra-tumoral CD56$^+$ cell counts averaged
338 across CT and PT regions were positively associated with DFS, but a similar association was not
339 significant for CD8$^+$ cell counts (**figure 2C,E**), consistent with our prior work showing that CD8
340 density across tumor, or in the invasive margins (ie, PT regions) was not correlated with patient
341 survival (10). Both CD8$^+$ and CD56$^+$ cells averaged between CT and PT independently corre-
342 sponded with OS (**figure 2D,F**). Similar trends were observed when considering CT and PT sep-
343 arately to varying degrees of statistical significance (**supplemental figures S4-S5**). Further as-
344 sessment revealed that simultaneous CD8$^+$ and CD56$^+$ counts above their medians were more
345 strongly associated with prolonged OS (**figure 2H**). Their joint impact on DFS was less striking,
346 but evident when considering density of CD8$^+$ and CD56$^+$ cells in CT only (**figure 2G, supple-**
347 **mental figure S6**). Observations from Kaplan-Meier analyses were consistent when adjusting for
348 patient age and sex in a Cox proportional hazards model, and statistical power was insufficient to
349 adjust for cancer stage and prior chemotherapy treatment (**supplemental table 1**). Collectively,
350 these data demonstrate that combined presence of NK cells and CD8 T cells predicts better OS,
351 pointing towards potential complementary antitumor activities.

352

353 **mIF imaging reveals the extent of MHC class I expression variation in patient resected**
354 **tumor tissues**. To further explore the relationship between lymphocyte infiltration and activation
355 and tumor cell MHC-I expression considering its vast heterogeneity in NSCLC and the increased
356 prognostic power observed with simultaneous infiltration of NK cells and CD8 T cells, we imple-
357 mented mIF imaging with combined spatial analysis of whole tumor sections.

358 Like the TMA analysis, we observed broadly variable MHC-I expression by mIF as shown
359 in representative SCC and AdenoCA images (**figure 3A**). Because our prior work demonstrated
360 that CD8 T cell infiltrations in NSCLC are highly heterogeneous across tumor regions (10), we
361 developed a tumor regional approach to delineate spatial relationships between NK cells, T cells
362 and tumor cell MHC-I expression in 3 mm^2 regions by tumor type (**supplemental figure S1, and**
363 **see Methods**). Cohort-wide MHC-I expression per region revealed total MHC-I loss in 26% of
364 regions and >90% loss in 47% of regions, with similar distributions observed in AdenoCA and
365 SCC (**figure 3B**). Wide-ranging inter- and intra-patient MHC-I expression variability was observed
366 with the mean expression per patient ranging from 0.1%-81% of panCK+ cells, and at least one
367 region per tumor displaying >40% MHC-I loss (**figure 3C**). Tumor cell MHC-I loss was thus com-
368 mon among NSCLC patients and heterogeneous across regions of tumor resections.

369

370 **Tumor cell MHC-I deficiency is associated with decreased NK and T cell presence and**
371 **activity in the NSCLC TME**. We next investigated how NK cell or CD8 T cell infiltration and
372 activation state corresponded to tumor cell MHC-I variability by building OPLSDA models to com-
373 pare the presence of T cells and NK cells in MHC-I-disparate tumor regions in AdenoCA (**figure**
374 **4A-D**) or SCC (**figure 4E-H**) tumors. Lymphocyte activation was inferred by IFNγ staining; though
375 IFNγ is a secreted cytokine and as such its source cannot be definitively determined by mIF, we
376 observed IFNγ most frequently in the presence of NK cells and T cells, indicative of activation
377 (**supplemental figure S7, figure 5**). Three tumors displayed strong IFNγ staining in tumor nests

378 lacking substantial lymphocyte infiltration, possibly indicative of a non-lymphocyte source of IFNγ
379 in these tumors.

380 Our resulting OPLSDA models were able to discriminate between tumor regions with high
381 and low MHC-I expression based on lymphocyte infiltrates with 79% (AdenoCA) or 87% (SCC)
382 accuracy, revealing distinct immune signatures of MHC-I high or low tumors (**figure 4A,E**). Vari-
383 able importance in projection (VIP) scores from the AdenoCA model revealed that stromal $CD3^{-}$
384 $CD56^{+}$ NK cells and as well as both stroma- and tumor-associated $CD56^{+}CD3^{+}$ cells were en-
385 riched in tumor regions with tumor MHC-I expression below the median, whereas tumor-associ-
386 ated $CD3^{+}CD8^{-}$ (putative CD4+) and $CD3^{+}CD8^{+}$ T cells were enriched in regions with MHC-I ex-
387 pression above the median (VIP > 1) (**figure 4B**). Tumor regions with high MHC-I expression also
388 displayed a greater density of $IFN\gamma^{+}$ CD8 T cells and NK cells (**figure 4D**), and Spearman corre-
389 lation analysis revealed that tumoral $IFN\gamma^{+}$ CD8 T cell densities were positively correlated with
390 $IFN\gamma^{+}$ NK cells in the stroma and tumor nest (**figure 4C,G, blue, bolded text**).

391 VIP scores from the SCC model indicated that $CD3^{+}CD8^{-}$ and $CD3^{+}CD8^{+}$ T cells, $CD3^{-}$
392 $CD56^{+}$ NK cells, and $CD56^{+}CD3^{+}$ cells were among the top features contributing to the separation
393 between MHC-I replete and deficient tumors (VIP > 1) (**figure 4F,H**). Akin with the adenocarcino-
394 mas, the only lymphocyte population found enriched in MHC-I low SCC tumor regions were $IFN\gamma^{-}$
395 stromal NK cells (**figure 4H**), indicating that inactive NK cells are abundant in the stroma of tumors
396 with MHC-I loss for both AdenoCA and SCC subtypes. We observed a clear lack of immune
397 infiltration into tumor nests with MHC-I loss in SCC tumors (**supplemental figure S8**). Addition-
398 ally, we observed significant negative pairwise correlations between $MHC\text{-}I^{-}$ tumor cell counts
399 and $IFN\gamma^{+}$ NK cells, $CD56^{+}CD3^{+}$ cells, $CD3^{+}CD8^{+}$ T cells, and $CD3^{+}CD8^{-}$ T cells, whereas stromal
400 $IFN\gamma^{-}$ NK cells were the only immune population positively correlated with $MHC\text{-}I^{-}$ cell densities
401 (**figure 4G**). This uniquely positive correlation further distinguishes the presence of NK cells in
402 the stroma of SCC tumors with substantial MHC-I downregulation. Together, these data indicate

403 that functional, tumor-infiltrating NK cells and T cells marked by IFNγ expression were best asso-
404 ciated with and coinhabited tumor regions expressing high MHC-I (**figure 4I**).

405

406 **Local neighborhood analysis of IFNγ$^+$ NK cells and CD8 T cells in the NSCLC TME reveals**
407 **tightly clustered lymphocytes marked by IFNγ staining near MHC-I± tumor cells.** Given the
408 observed differences in lymphocyte presence in MHC-I-disparate NSCLC tumors, we questioned
409 whether IFNγ$^+$ NK cells and CD8 T cells differ from IFNγ$^-$ lymphocytes with respect to their prox-
410 imity to other immune cells and MHC-I expressing tumor cells. To uncover potential functional
411 differences in cell-cell communication between activated NK cells and CD8 T cells, we determined
412 the cellular neighborhood profile of these effector cell types using spatial, cell-centric analyses of
413 the mIF images (**supplemental figure S2**). The cellular neighborhood profile scores of both tu-
414 mor- and stroma-associated cells were input into an OPLSDA model to delineate colocalization
415 differences between IFNγ± NK cells (**figure 6A-C**) and IFNγ± CD8 T cells (**figure 6E-G**). Both
416 models accurately distinguished between IFNγ$^+$ and IFNγ$^-$ lymphocytes based on their neighbor-
417 hood profiles with cross-validation accuracy scores of 96% and 97%, respectively (**figure 6A,E**).
418 Comparing the two models, we observed that both IFNγ$^+$ NK cells and CD8 T cells associated
419 with all IFNγ$^+$ lymphocyte subsets more so than IFNγ$^-$ cells (**figure 6B,F**). In agreement with our
420 regional analyses (**figure 4**), we found that NK cells and CD8 T cells were more likely to be IFNγ$^+$
421 in the tumor as opposed to the surrounding stroma (**figure 6D,H**). Moreover, we observed that
422 IFNγ$^+$ NK cells and IFNγ$^+$ CD8 T cells in the tumor nests colocalized with MHC-I$^+$ tumor cells more
423 frequently than did IFNγ$^-$ lymphocytes, suggesting preferential localization of activated cells to
424 tumors with MHC-I expression (**figure 6D,H**). Strikingly, IFNγ$^+$ NK cells and CD8 T cells were
425 more frequently associated with MHC-I$^-$ tumor cells compared to their IFNγ$^-$ counterparts, indi-
426 cating infiltration of IFNγ-secreting lymphocytes into both MHC-I$^+$ and MHC-I$^-$ tumor nests (**figure**
427 **6I**). To validate these observations over larger radii (<200 μm), we quantified the number of r-

428 neighbors—i.e., the number of neighbors in radius r around a center cell (37). We observed IFNγ$^+$
429 CD8 T cells had fewer MHC-I$^-$ neighbors than MHC-I$^+$ neighbors, and their association with MHC-
430 I$^-$ tumor cells was less than what was expected by random chance (**figure 6J**). This may signify
431 deliberate enrichment of IFNγ$^+$ CD8 T cells in MHC-I-bearing tumors. In contrast, IFNγ$^+$ NK cells
432 associated similarly with MHC-I$^+$ and MHC-I$^-$ tumor cells, suggesting that NK cells may become
433 or remain activated in the MHC-I-deficient TME. Marked colocalization of IFNγ$^+$ NK cells with other
434 IFNγ$^+$ lymphocytes including NK cells, CD8$^-$ T cells, and CD8$^+$ T cells additionally suggests that
435 lymphocytes may be activated en masse in MHC-I-bearing tumor regions that can trigger NK cell
436 activation. IFNγ produced in these clusters of activated lymphocytes thus may be indicative of
437 type I immune responses in the TME.

438

439 **DISCUSSION**

440 While targeting immune checkpoints with CPI has had a substantive impact on the treatment of
441 NSCLC, a minority of patients display durable responses. Whether this is due to hindered immune
442 infiltration, functional exhaustion, tumor cell evasion of immune recognition by loss of MHC-I ex-
443 pression, or alternative mechanisms remains to be determined. Understanding the basis of this
444 selectivity will increase the appropriate targeting of CPI or combination therapies to patients most
445 likely to benefit and will ultimately lead to development of innovative approaches to expand the
446 proportion of patients who receive clinical benefit.

447 We hypothesized that coordinated activities of both CD8 T cells and NK cells may jointly
448 enhance targeted lysis of NSCLC tumor cells while preventing tumor cell MHC-I loss. We ana-
449 lyzed resected patient (non-CPI treated) tumor tissues by both traditional IHC and mIF to simul-
450 taneously probe NK cells and CD8 T cells *in situ*, their effector activity indicated by IFNγ staining,
451 and their co-localization in MHC-I disparate NSCLC tumors. To define differences in lymphocyte
452 activation and intercellular communication in tumors with and without MHC-I expression, we

453 leveraged the inherent heterogeneity of the TME by developing a suite of spatial analysis methods
454 spanning whole tumors, tumor sub-regions, and single-cell enumeration of NK cell and T cell
455 neighborhoods. This use of integrative systems consistently pointed towards coordinated anti-
456 tumor activity of NK cells and T cells, particularly in tumors with MHC-I expression.

457 Consistent with prior work (23, 25, 28, 30), both cohorts displayed stark inter-patient and
458 intra-tumoral heterogeneity in MHC-I expression. Although MHC-I loss can lead to the develop-
459 ment of $CD8^+$ T cell refractory tumors, we did not observe an association between tumor cell
460 MHC-I expression and NSCLC patient survival in this study. Others have speculated cohort-spe-
461 cific composition, clinicopathologic characteristics, genetic contribution and/or survival/events
462 may obfuscate any potential association (28-30). MHC-I loss thus may indirectly impact patient
463 survival by regulating lymphocyte occupancy and activation.

464 IHC analysis of Cohort 1 revealed that tumors with high counts of both $CD8^+$ and $CD56^+$
465 cells were more strongly associated with OS compared to tumors with high $CD56^+$ or $CD8^+$ cells
466 only. Using mIF to concurrently enumerate NK cell and CD8 T cell infiltrates in Cohort 2, we
467 observed positively correlated tumor-infiltrating NK cells and CD8 T cells with greater densities in
468 tumor nests expressing high levels of MHC-I, indicating coordinated infiltration. Furthermore, spa-
469 tial analysis of local cellular neighborhoods revealed infiltrated NK and CD8 T cells are present in
470 clusters marked by IFNγ activity together with $CD8^-$ T cells. Though much less frequent, similar
471 immune clusters were observed in tumors with MHC-I loss, suggesting that an effector response
472 involving NK cells, CD8 T cells, and $CD8^-$ T cells can be active, and possibly leveraged, even in
473 a setting considered refractory to lymphocyte immune control.

474 Whether intra-tumoral IFNγ promotes tumor cell MHC-I expression, immune recruitment
475 and co-localization, or coordinate lymphocyte effector activity awaits further analysis, but these
476 findings suggest that CPI plus novel approaches designed to jointly elicit NK and T cell effector
477 activities may be key to developing next generation immunotherapies. Antigen-stimulated NK

478 cells have been shown to provide support to CD8 T cell antitumor immunity in a mouse model of
479 lung adenocarcinoma (14). Likewise, human induced pluripotent stem cell (iPSC-)derived NK
480 cells have been shown to enhance T cell recruitment and activation to tumors, coinciding with
481 improved T cell sensitivity to CPI and enhanced antitumor control (40). Cytokine activation can
482 additionally invigorate NK cells to curb or regress tumor outgrowth, even in MHC-I^{-} tumors (17).
483 The potential benefit of NK cells in NSCLC is bolstered by prior work that showed that human NK
484 cell cytolytic activity is associated with lower cancer risk (41), whereas NK cell deficiency is asso-
485 ciated with increased cancer risk (42-44). Our data contrast recent observations in soft tissue
486 sarcoma that CD56^{+} NK cell infiltrates indicate a poor prognosis and do not colocalize with CD8
487 T cells or MHC-I^{+} tumor cells, indicating that the role of NK cells suggested by our results may be
488 context specific (45). This apparent synergy between NK cells and cytotoxic T cells in the NSCLC
489 TME highlights a vital clinical value in developing CPI treatments which stimulate both lymphocyte
490 populations.

491 Our findings that NK cells had infiltrated into tumor nests and displayed evidence of IFNγ
492 activity in NSCLC begs the question, why might tumoral NK cells become ineffective drivers of
493 anti-tumor immunity? Emerging evidence suggests that NK cell activity may be hindered in the
494 lung cancer TME. Human NKp46^{+} NK cells were shown to infiltrate the invasive margin of lung
495 tissue stroma surrounding tumor nests in NSCLC patients with no apparent effect on clinical out-
496 comes (33). These intra-tumoral NK cells displayed inferior effector activities in comparison to
497 their counterpart NK cells in peripheral blood (33). Whether due to suppressive mechanisms as-
498 sociated with the lung environment itself (46) or more direct suppression via tumor cells remains
499 unresolved as cancer cells can downregulate or secrete NK receptor ligands to evade natural
500 killing, and the TME is rife with suppressive factors which can impede NK cell activity (47). Prior
501 work in mouse models has further shown NK cells also undergo disarming in MHC-I^{-} tumors
502 rendering them hyporesponsive and unable to mediate tumor cell clearance (17, 48). As our study

503 affirms the significant association with survival and notable infiltration into MHC-I$^+$ tumor nests of
504 NK cells in NSCLC, future studies are needed to uncover the root causes of NK cell disarming in
505 the lung cancer TME to fully realize their potential as anti-tumor effectors.

506 Though these multifaceted spatial analyses consistently revealed NK cell and CD8 T cell
507 co-occurrence within NSCLC tumors, there are several limitations to consider. The TMA data from
508 Cohort 1 were manually generated by a pathologist and consequently may be impacted by sub-
509 jective bias; however, this concern is mitigated as automated analysis yielded similar results. mIF
510 imaging was limited to six phenotypic markers plus nuclear staining, thus constraining analysis of
511 the full complexity of the tumor-associated immune milieu. Consequently, we relied on IFNγ ex-
512 pression as a marker of lymphocyte activity and were unable to test for expression of other cyto-
513 toxic markers and inhibitory ligands which may obscure true activity levels of cytotoxic T cells and
514 NK cells. Ongoing work with higher dimensional imaging (e.g., spatial transcriptomics) will provide
515 a more comprehensive view of immune cell diversity, occupancy, proliferation, and activation in
516 the TME. As IFNγ is a secreted cytokine, we were unable to definitively determine its source.
517 Nevertheless, analysis of our data without three select tumors that displayed strong IFNγ staining
518 in the absence of lymphocytes yielded similar results and thus non-lymphocyte IFNγ was not a
519 major confounder.

520 Another important limitation of our study is that the cohort was composed of only complete
521 resections and thus there was no opportunity assess tissue after chemotherapy or immunother-
522 apy treatment. For instance, it remains to be determined whether NK cells drive treatment-related
523 recruitment and/or activation of CD8 T cells in the TME, or vice versa. Likewise, whether stark
524 differences in lymphocyte populations and activity in tumors with loss of MHC-I expression results
525 from differences in lymphocyte infiltration, expansion, or retention in the TME remains unclear.
526 Other outstanding questions include whether patient tumors are infiltrated by circulating NK cells
527 with higher baseline cytotoxic activity, by lung resident NK cells with lower baseline cytotoxic

activity, or both. Whether these different types of NK cells could affect other tumor-infiltrating immune cells, such as helper T cells, and whether there are specific interactions that either cause or arise from the spatial associations observed in the data remains to be determined. Future mechanistic studies in animal models will help to delineate the effect of MHC-I on the balance of NK cells and their impact on the tumor-immune landscape.

Notwithstanding these challenges, we have shown that tumor cell MHC-I loss is common in NSCLC patient tissues across two separate cohorts, an effect that negatively impacted lymphocyte occupancy and activity in the TME. While we did not find MHC-I to be predictive of patient survival, CD8+ and CD56+ cells were independently associated with survival and had an increased effect in tumors with simultaneously high CD8+ and CD56+ counts. This evidence of lymphocyte activation and intercellular communication in the presence of MHC-I^{+} NSCLC tumors highlights both the vital importance and promise for developing novel immunotherapies that leverage both NK cells and CD8 T cells to enhance immunologic control of NSCLC.

REFERENCES

1. Molina JR, Yang P, Cassivi SD, Schild SE, Adjei AA. Non-small cell lung cancer: epidemiology, risk factors, treatment, and survivorship. Mayo Clinic proceedings. 2008;83(5):584-94.
2. Siegel RL, Miller KD, Fuchs HE, Jemal A. Cancer statistics, 2022. CA: a cancer journal for clinicians. 2022;72(1):7-33.
3. Chen Z, Fillmore CM, Hammerman PS, Kim CF, Wong KK. Non-small-cell lung cancers: a heterogeneous set of diseases. Nat Rev Cancer. 2014;14(8):535-46.
4. Travis WD, Brambilla E, Noguchi M, Nicholson AG, Geisinger K, Yatabe Y, et al. International Association for the Study of Lung Cancer/American Thoracic Society/European Respiratory Society: international multidisciplinary classification of lung adenocarcinoma: executive summary. Proc Am Thorac Soc. 2011;8(5):381-5.
5. Stankovic B, Bjorhovde HAK, Skarshaug R, Aamodt H, Frafjord A, Muller E, et al. Immune Cell Composition in Human Non-small Cell Lung Cancer. Frontiers in immunology. 2018;9:3101.
6. Geng Y, Shao Y, He W, Hu W, Xu Y, Chen J, et al. Prognostic Role of Tumor-Infiltrating Lymphocytes in Lung Cancer: a Meta-Analysis. Cellular physiology and biochemistry : international journal of experimental cellular physiology, biochemistry, and pharmacology. 2015;37(4):1560-71.

561 7. Zeng DQ, Yu YF, Ou QY, Li XY, Zhong RZ, Xie CM, et al. Prognostic and predictive
562 value of tumor-infiltrating lymphocytes for clinical therapeutic research in patients with
563 non-small cell lung cancer. Oncotarget. 2016;7(12):13765-81.
564 8. Schalper KA, Brown J, Carvajal-Hausdorf D, McLaughlin J, Velcheti V, Syrigos KN,
565 et al. Objective measurement and clinical significance of TILs in non-small cell lung
566 cancer. J Natl Cancer Inst. 2015;107(3).
567 9. Esendagli G, Bruderek K, Goldmann T, Busche A, Branscheid D, Vollmer E, et al.
568 Malignant and non-malignant lung tissue areas are differentially populated by natural killer
569 cells and regulatory T cells in non-small cell lung cancer. Lung cancer. 2008;59(1):32-40.
570 10. Obeid JM, Wages NA, Hu Y, Deacon DH, Slingluff CL, Jr. Heterogeneity of CD8(+)
571 tumor-infiltrating lymphocytes in non-small-cell lung cancer: impact on patient prognostic
572 assessments and comparison of quantification by different sampling strategies. Cancer
573 immunology, immunotherapy : CII. 2017;66(1):33-43.
574 11. Federico L, McGrail DJ, Bentebibel SE, Haymaker C, Ravelli A, Forget MA, et al.
575 Distinct tumor-infiltrating lymphocyte landscapes are associated with clinical outcomes in
576 localized non-small-cell lung cancer. Annals of oncology : official journal of the European
577 Society for Medical Oncology. 2022;33(1):42-56.
578 12. Guillerey C, Huntington ND, Smyth MJ. Targeting natural killer cells in cancer
579 immunotherapy. Nat Immunol. 2016;17(9):1025-36.
580 13. Malmberg KJ, Carlsten M, Bjorklund A, Sohlberg E, Bryceson YT, Ljunggren HG.
581 Natural killer cell-mediated immunosurveillance of human cancer. Semin Immunol.
582 2017;31:20-9.
583 14. Schmidt L, Eskiocak B, Kohn R, Dang C, Joshi NS, DuPage M, et al. Enhanced
584 adaptive immune responses in lung adenocarcinoma through natural killer cell
585 stimulation. Proc Natl Acad Sci U S A. 2019;116(35):17460-9.
586 15. Liu RB, Engels B, Arina A, Schreiber K, Hyjek E, Schietinger A, et al. Densely
587 granulated murine NK cells eradicate large solid tumors. Cancer research.
588 2012;72(8):1964-74.
589 16. Nicolai CJ, Wolf N, Chang IC, Kirn G, Marcus A, Ndubaku CO, et al. NK cells
590 mediate clearance of CD8(+) T cell-resistant tumors in response to STING agonists.
591 Science immunology. 2020;5(45).
592 17. Ardolino M, Azimi CS, Iannello A, Trevino TN, Horan L, Zhang L, et al. Cytokine
593 therapy reverses NK cell anergy in MHC-deficient tumors. J Clin Invest.
594 2014;124(11):4781-94.
595 18. Bottcher JP, Bonavita E, Chakravarty P, Blees H, Cabeza-Cabrerizo M,
596 Sammicheli S, et al. NK Cells Stimulate Recruitment of cDC1 into the Tumor
597 Microenvironment Promoting Cancer Immune Control. Cell. 2018;172(5):1022-37 e14.
598 19. Kyrysyuk O, Wucherpfennig KW. Designing Cancer Immunotherapies That
599 Engage T Cells and NK Cells. Annu Rev Immunol. 2023;41:17-38.
600 20. Topalian SL, Hodi FS, Brahmer JR, Gettinger SN, Smith DC, McDermott DF, et al.
601 Safety, activity, and immune correlates of anti-PD-1 antibody in cancer. The New England
602 journal of medicine. 2012;366(26):2443-54.
603 21. Brahmer JR, Tykodi SS, Chow LQ, Hwu WJ, Topalian SL, Hwu P, et al. Safety and
604 activity of anti-PD-L1 antibody in patients with advanced cancer. The New England
605 journal of medicine. 2012;366(26):2455-65.

606 22. Santarpia M, Giovannetti E, Rolfo C, Karachaliou N, Gonzalez-Cao M, Altavilla G,
607 et al. Recent developments in the use of immunotherapy in non-small cell lung cancer.
608 Expert Rev Respir Med. 2016;10(7):781-98.
609 23. Garrido F, Aptsiauri N, Doorduijn EM, Garcia Lora AM, van Hall T. The urgent need
610 to recover MHC class I in cancers for effective immunotherapy. Current opinion in
611 immunology. 2016;39:44-51.
612 24. Thunnissen E, van der Oord K, den Bakker M. Prognostic and predictive
613 biomarkers in lung cancer. A review. Virchows Arch. 2014;464(3):347-58.
614 25. Redondo M, Ruiz-Cabello F, Concha A, Cabrera T, Perez-Ayala M, Oliva MR, et
615 al. Altered HLA class I expression in non-small cell lung cancer is independent of c-myc
616 activation. Cancer research. 1991;51(9):2463-8.
617 26. Korkolopoulou P, Kaklamanis L, Pezzella F, Harris AL, Gatter KC. Loss of antigen-
618 presenting molecules (MHC class I and TAP-1) in lung cancer. British journal of cancer.
619 1996;73(2):148-53.
620 27. Delp K, Momburg F, Hilmes C, Huber C, Seliger B. Functional deficiencies of
621 components of the MHC class I antigen pathway in human tumors of epithelial origin.
622 Bone Marrow Transplant. 2000;25 Suppl 2:S88-95.
623 28. Ramnath N, Tan D, Li Q, Hylander BL, Bogner P, Ryes L, et al. Is downregulation
624 of MHC class I antigen expression in human non-small cell lung cancer associated with
625 prolonged survival? Cancer immunology, immunotherapy : CII. 2006;55(8):891-9.
626 29. Li X, Guo F, Liu Y, Chen HJ, Wen F, Zou B, et al. NLRC5 expression in tumors
627 and its role as a negative prognostic indicator in stage III non-small-cell lung cancer
628 patients. Oncol Lett. 2015;10(3):1533-40.
629 30. Datar IJ, Hauc SC, Desai S, Gianino N, Henick B, Liu Y, et al. Spatial Analysis and
630 Clinical Significance of HLA Class-I and Class-II Subunit Expression in Non-Small Cell
631 Lung Cancer. Clinical cancer research : an official journal of the American Association for
632 Cancer Research. 2021;27(10):2837-47.
633 31. Kikuchi E, Yamazaki K, Torigoe T, Cho Y, Miyamoto M, Oizumi S, et al. HLA class
634 I antigen expression is associated with a favorable prognosis in early stage non-small cell
635 lung cancer. Cancer Sci. 2007;98(9):1424-30.
636 32. Vivier E, Raulet DH, Moretta A, Caligiuri MA, Zitvogel L, Lanier LL, et al. Innate or
637 adaptive immunity? The example of natural killer cells. Science. 2011;331(6013):44-9.
638 33. Platonova S, Cherfils-Vicini J, Damotte D, Crozet L, Vieillard V, Validire P, et al.
639 Profound coordinated alterations of intratumoral NK cell phenotype and function in lung
640 carcinoma. Cancer research. 2011;71(16):5412-22.
641 34. Erdag G, Schaefer JT, Smolkin ME, Deacon DH, Shea SM, Dengel LT, et al.
642 Immunotype and immunohistologic characteristics of tumor-infiltrating immune cells are
643 associated with clinical outcome in metastatic melanoma. Cancer research.
644 2012;72(5):1070-80.
645 35. Stam NJ, Spits H, Ploegh HL. Monoclonal antibodies raised against denatured
646 HLA-B locus heavy chains permit biochemical characterization of certain HLA-C locus
647 products. J Immunol. 1986;137(7):2299-306.
648 36. Mauldin IS, Mahmutovic A, Young SJ, Slingluff CL, Jr. Multiplex
649 Immunofluorescence Histology for Immune Cell Infiltrates in Melanoma-Associated
650 Tertiary Lymphoid Structures. Methods Mol Biol. 2021;2265:573-87.

651 37. Baddeley A, Turner R. spatstat: An R Package for Analyzing Spatial Point
652 Patterns. . Journal of Statistical Software. 2005;12:1-42.
653 38. Dolatshahi S, Butler AL, Siedner MJ, Ngonzi J, Edlow AG, Adong J, et al. Altered
654 Maternal Antibody Profiles in Women With Human Immunodeficiency Virus Drive
655 Changes in Transplacental Antibody Transfer. Clinical infectious diseases : an official
656 publication of the Infectious Diseases Society of America. 2022;75(8):1359-69.
657 39. Grace PS, Dolatshahi S, Lu LL, Cain A, Palmieri F, Petrone L, et al. Antibody
658 Subclass and Glycosylation Shift Following Effective TB Treatment. Frontiers in
659 immunology. 2021;12:679973.
660 40. Cichocki F, Bjordahl R, Gaidarova S, Mahmood S, Abujarour R, Wang H, et al.
661 iPSC-derived NK cells maintain high cytotoxicity and enhance in vivo tumor control in
662 concert with T cells and anti-PD-1 therapy. Science translational medicine. 2020;12(568).
663 41. Imai K, Matsuyama S, Miyake S, Suga K, Nakachi K. Natural cytotoxic activity of
664 peripheral-blood lymphocytes and cancer incidence: an 11-year follow-up study of a
665 general population. Lancet. 2000;356(9244):1795-9.
666 42. Orange JS. Natural killer cell deficiency. The Journal of allergy and clinical
667 immunology. 2013;132(3):515-25.
668 43. Moon WY, Powis SJ. Does Natural Killer Cell Deficiency (NKD) Increase the Risk
669 of Cancer? NKD May Increase the Risk of Some Virus Induced Cancer. Frontiers in
670 immunology. 2019;10:1703.
671 44. Mace EM, Orange JS. Emerging insights into human health and NK cell biology
672 from the study of NK cell deficiencies. Immunol Rev. 2019;287(1):202-25.
673 45. Cruz SM, Sholevar CJ, Judge SJ, Darrow MA, Iranpur KR, Farley LE, et al.
674 Intratumoral NKp46(+) natural killer cells are spatially distanced from T and MHC-I(+)
675 cells with prognostic implications in soft tissue sarcoma. Frontiers in immunology.
676 2023;14:1230534.
677 46. Marquardt N, Kekalainen E, Chen P, Kvedaraite E, Wilson JN, Ivarsson MA, et al.
678 Human lung natural killer cells are predominantly comprised of highly differentiated
679 hypofunctional CD69(-)CD56(dim) cells. The Journal of allergy and clinical immunology.
680 2017;139(4):1321-30 e4.
681 47. Granzin M, Wagner J, Kohl U, Cerwenka A, Huppert V, Ullrich E. Shaping of
682 Natural Killer Cell Antitumor Activity by Ex Vivo Cultivation. Frontiers in immunology.
683 2017;8:458.
684 48. Marcus A, Mao AJ, Lensink-Vasan M, Wang L, Vance RE, Raulet DH. Tumor-
685 Derived cGAMP Triggers a STING-Mediated Interferon Response in Non-tumor Cells to
686 Activate the NK Cell Response. Immunity. 2018;49(4):754-63 e4.
687

688

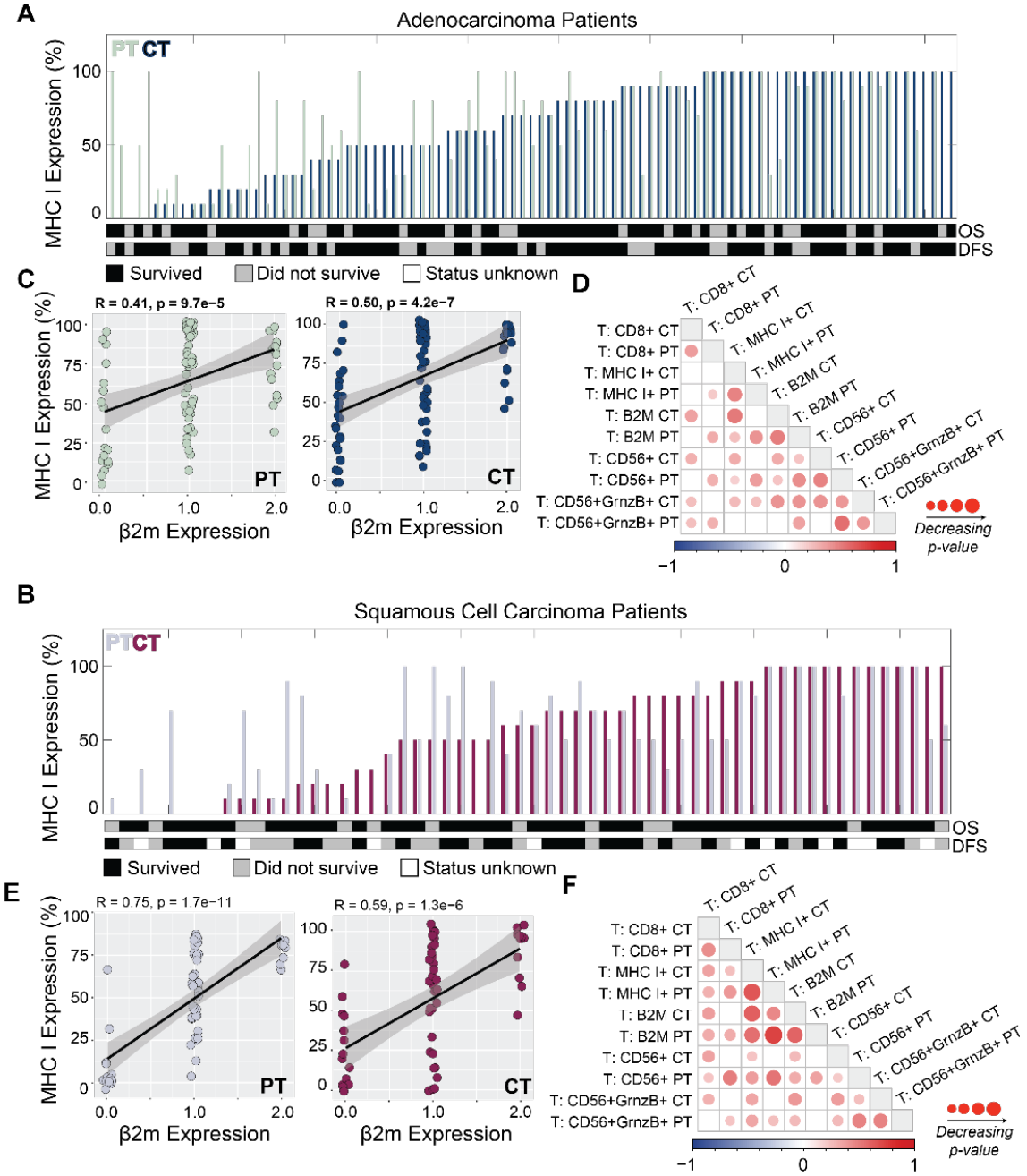

Figure 1. MHC class I expression in NSCLC exhibits intra- and inter-tumor heterogeneity and correlates with intra-tumoral lymphocytes. (A & B) MHC-I is variably expressed in tumors and across AdenoCA **(A)** and SCC **(B)** patients from Cohort 1. Bar plots represent the percent of tumoral MHC-I$^+$ cells per patient in the central tumor (CT) and peripheral tumor (PT). OS (overall survival) and DFS (disease-free survival) are shown for each patient below the bar graphs (black, survived; gray, did not survive; white, data not available). **(C & E)** β2M expression (0, low; 1, moderate; 2, high) in PT (left) and CT (right) correlates positively with MHC-I expression in AdenoCA **(C)** and SCC **(E)** patients from Cohort 1. R, Spearman correlation coefficient. **(D & F)** The correlation heatmaps show Spearman correlations between all features from Cohort 1 in AdenoCA **(D)** and SCC **(F)** patients. Circle color is proportional to correlation strength, and circle radius is proportional to significance. Insignificant correlations ($p > 0.05$) are indicated by white shading, and identity correlations are indicated with light grey.

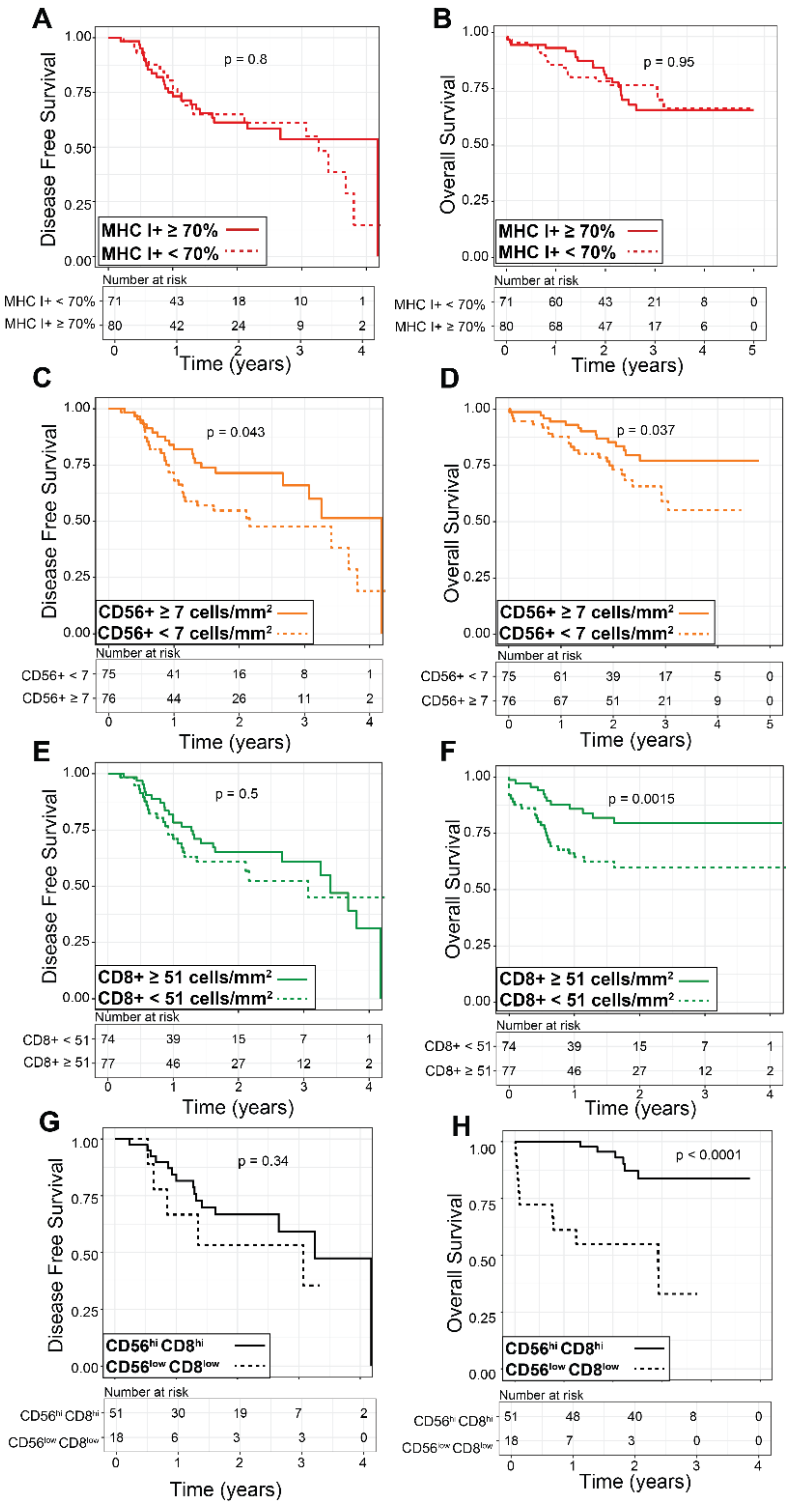

Figure 2. Probability of survival increases with increasing intra-tumoral CD8⁺ and CD56⁺ lymphocytes. Kaplan-Meier analysis predicts the probability of DFS or OS in Cohort 1 patients with respect to intra-tumoral MHC-I expression level **(A & B)**, CD56⁺ cell counts **(C & D)**, CD8⁺ cell counts **(E & F)**, or coincident CD56⁺ and CD8⁺ cell counts **(G & H)** above and below the median averaged between CT and PT regions. Significance was determined by a log-rank test.

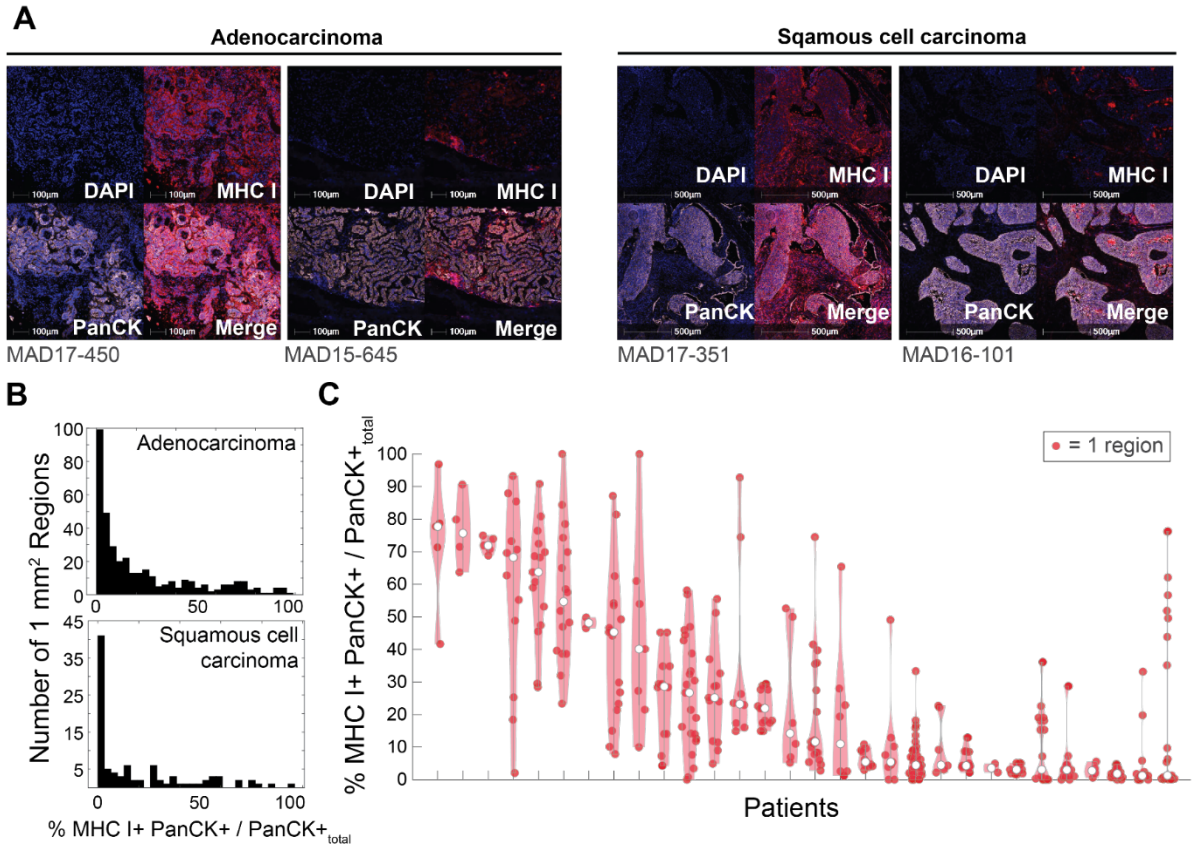

Figure 3. mIF imaging reveals extent of MHC class I expression variation in resected patient tumor tissues. (A) The representative images show an example of MHC-I loss in AdenoCA (left) and SCC (right). A representative image classified as MHC-I high or low (stratified at the median count of panCK+MHC-I+ tumor cells) is show for each tumor type. **(B & C)** The histograms show percentage of MHC-I+ tumor cells in each region in adenocarcinoma (top) and SCC (bottom) patients from Cohort 2. Percentages are defined as the number of MHC-I+ PanCK+ cells per total PanCK+ cells. **(C)** The violin plots show the percentage of MHC-I+ tumor cells per region for each patient where each dot represents a region and the white circles represent mean of all regions from a patient. Patients are sorted by average percentage of MHC-I+ cells across their regions. AdenoCA and SCC patients are both shown.

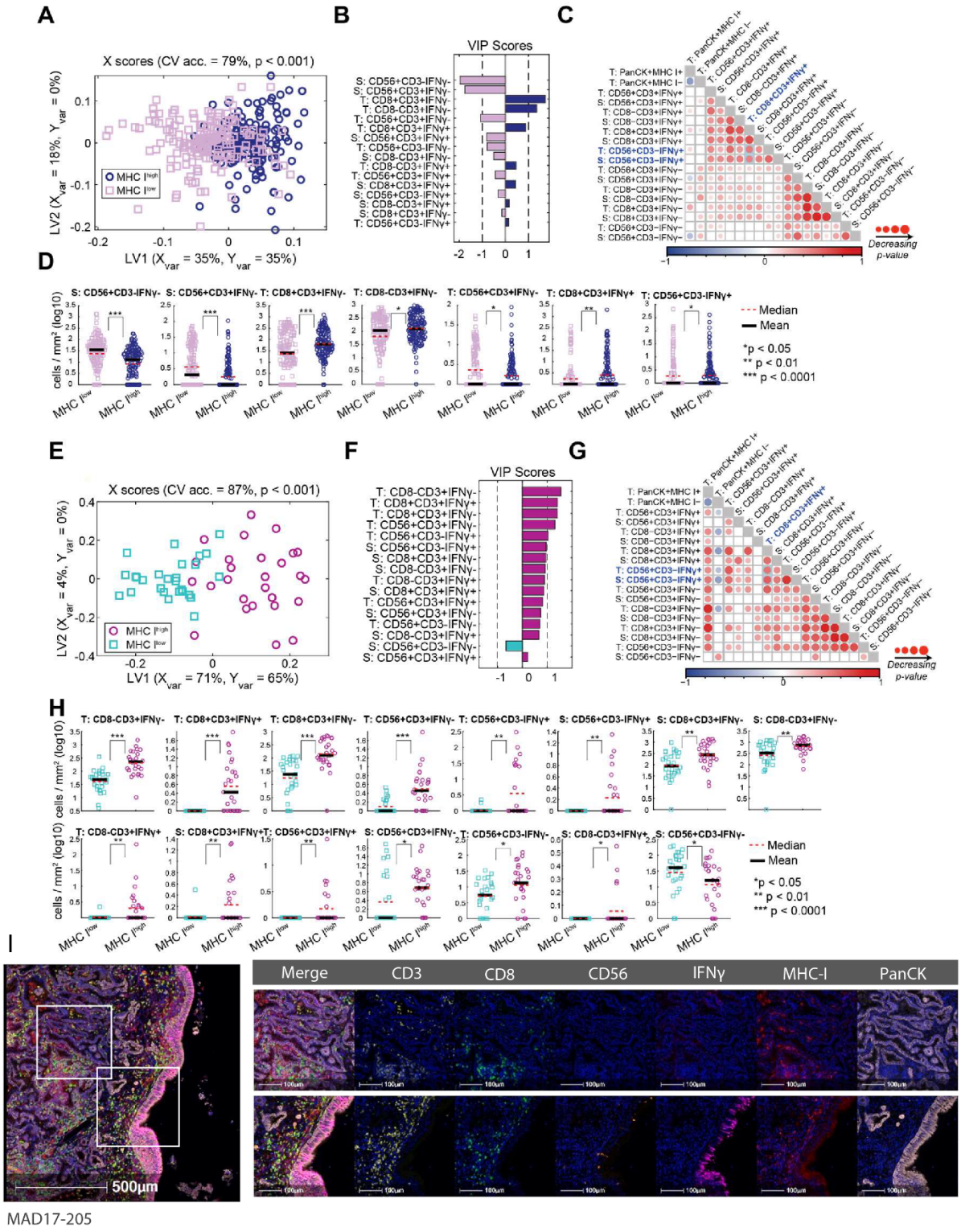
A
X scores (CV acc. = 79%, p < 0.001)
LV2 (Xvar = 18%, Yvar = 0%)
LV1 (Xvar = 35%, Yvar = 35%)
MHC Ihigh
MHC Ilow
B
VIP Scores
C
Decreasing p-value
D
cells / mm² (log10)
Median
Mean
*p < 0.05
** p < 0.01
*** p < 0.0001
E
X scores (CV acc. = 87%, p < 0.001)
LV2 (Xvar = 4%, Yvar = 0%)
LV1 (Xvar = 71%, Yvar = 65%)
F
VIP Scores
G
Decreasing p-value
H
cells / mm² (log10)
Median
Mean
*p < 0.05
** p < 0.01
*** p < 0.0001
I
Merge
CD3
CD8
CD56
IFNγ
MHC-I
PanCK
500µm
MAD17-205

718

Figure 4. Tumor infiltrated lymphocytes and IFNγ expression are associated with high tumor cell MHC-I expression. An OPLSDA model was constructed to discriminate between tumor regions with high or low MHC-I expression, defined as regions with MHC-I$^+$ tumor cell densities (cells/mm^2 classified tumor) above or below the cohort median in **(A-D)** AdenoCA and **(E-H)** SCC. A 5-fold cross validation yielded models with 79% (adenocarcinoma) and 87% (SCC) classification accuracy. Both models outperformed all of 1000 randomly permuted models ($p < 0.001$). **(A & E)** The scatter plots show the X scores, where each point represents one tumor region. LV1 & LV2, latent variable 1 and 2. **(B & F)** The bar plots show the Variable Importance in Projection (VIP) scores, artificially oriented in the direction of loadings on LV1 and colored according to their association with MHC-I high or MHC-I low regions. |VIP score| > 1 indicates a variable with greater than average influence on the separation between groups. **(C & G)** The correlation heatmaps show the Spearman correlations among immunologic features in tumor (T) and stroma (S) regions. Color intensity indicates correlation coefficient, and the circle size is inversely proportional to the p value. Insignificant correlations ($p > 0.05$) are indicated by white shading, and identity correlations are indicated with light grey. **(D & H)** The scatter plots show univariate comparisons between model features determined by a non-parametric Wilcoxon rank sum test followed by multiple comparison correction using the Benjamini-Hochberg method (*, $p < 0.05$; **, $p < 0.01$; *** $p < 0.0001$). Only features with an adjusted $p < 0.05$ are shown. **(I)** Representative image shows variation in lymphocyte occupancy and IFNγ staining in different regions of the same tumor that do not express (top) or express (bottom) MHC-I.

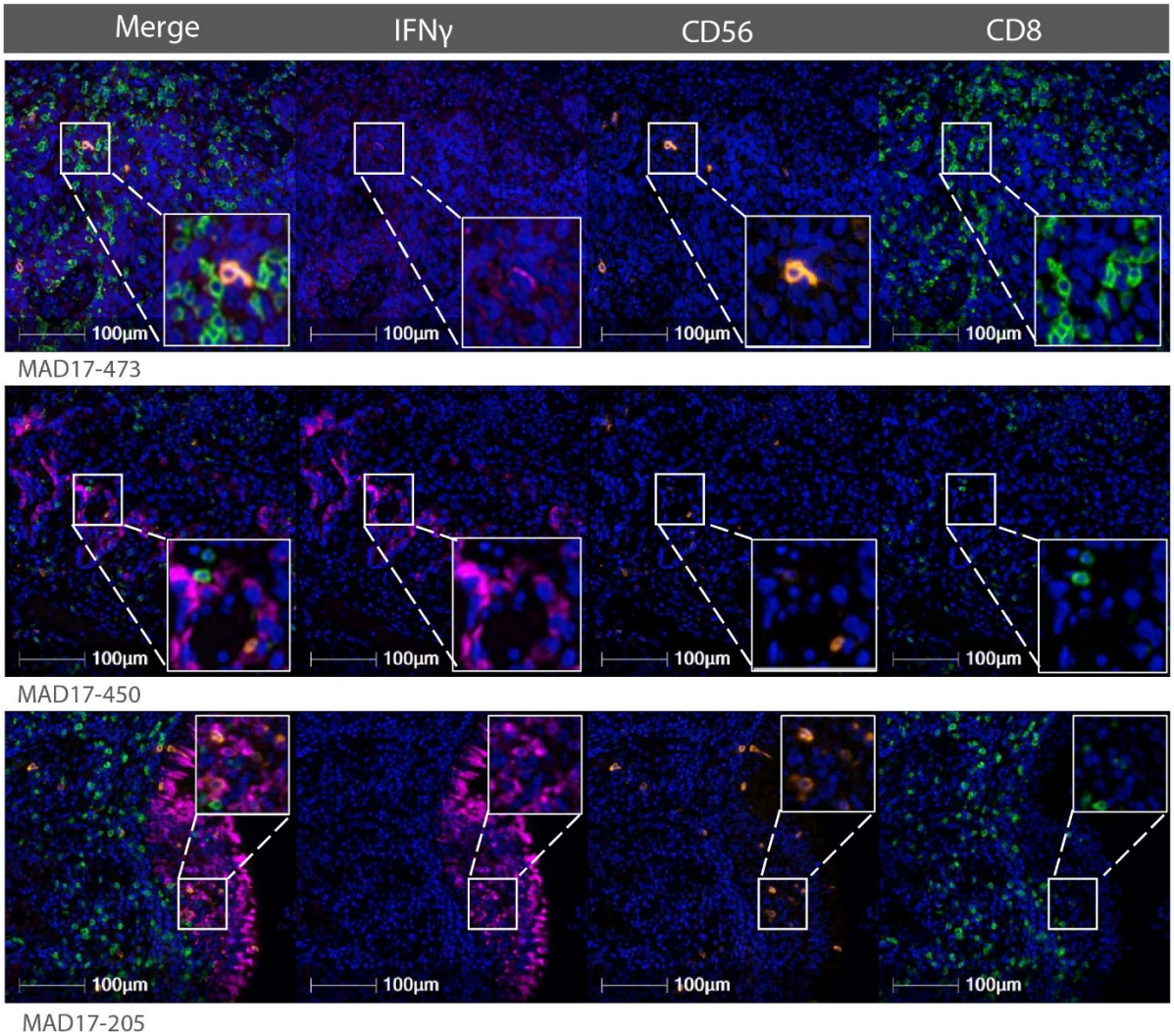

Figure 5. NK cells and CD8 T cells colocalize in areas with high IFNγ staining. The mIF images show representative instances of $CD56^{+}CD3^{-}$ NK cells and $CD3^{+}CD8^{+}$ T cells clustered together with evidence of IFNγ staining. Each row is drawn from a different patient tumor tissue. The box inset highlights instances of NK cell and CD8 T cell colocalization.

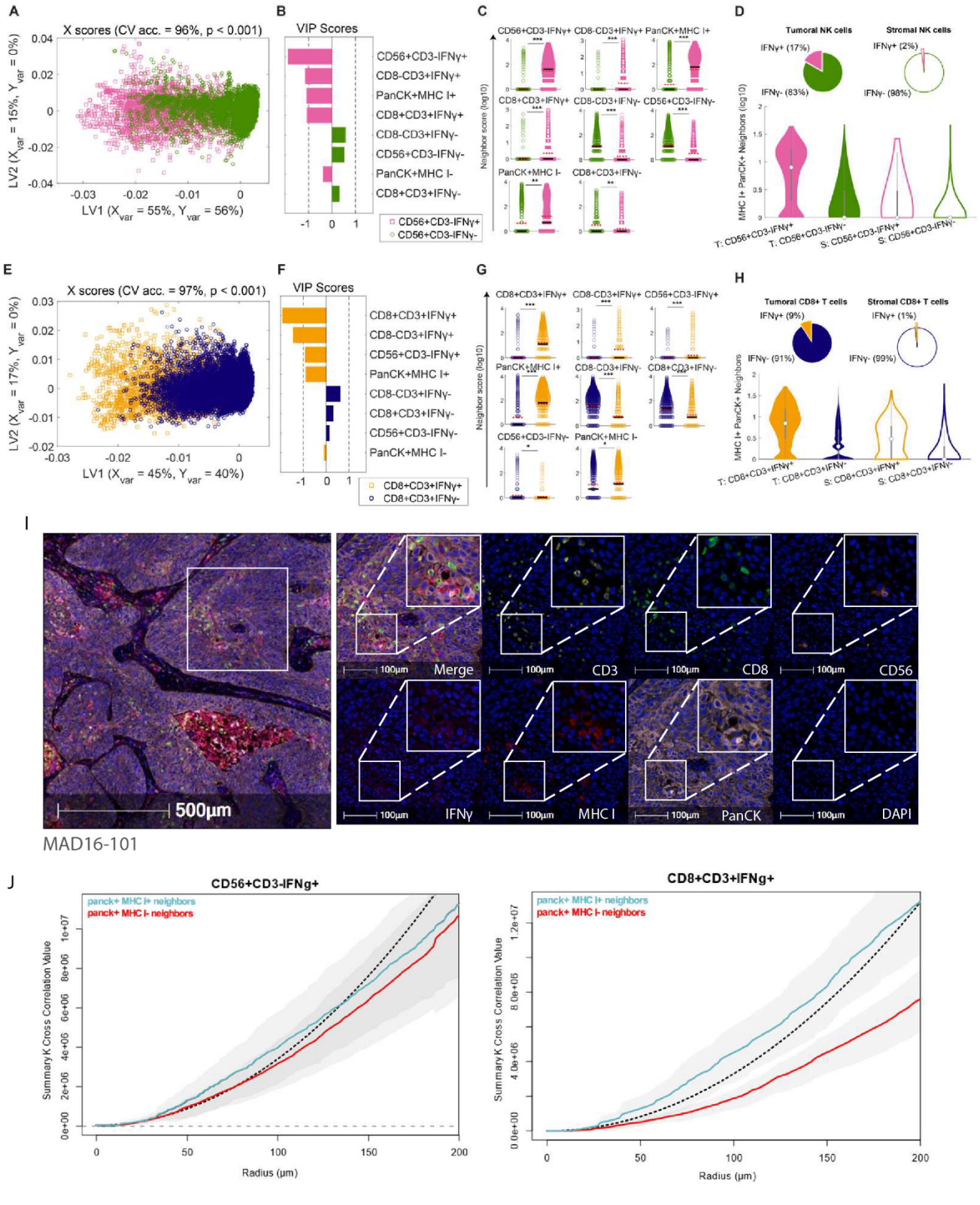
A
X scores (CV acc. = 96%, p < 0.001)
LV2 (Xvar = 15%, Yvar = 0%)
LV1 (Xvar = 55%, Yvar = 56%)
B
VIP Scores
CD56+CD3-IFNγ+
CD8-CD3+IFNγ+
PanCK+MHC I+
CD8+CD3+IFNγ+
CD8-CD3+IFNγ-
CD56+CD3-IFNγ-
PanCK+MHC I-
CD8+CD3+IFNγ-
CD56+CD3-IFNγ+
CD56+CD3-IFNγ-
C
Neighbor score (log10)
D
Tumoral NK cells
Stromal NK cells
IFNγ+ (17%)
IFNγ- (83%)
IFNγ+ (2%)
IFNγ- (98%)
MHC I+ PanCK+ Neighbors (log10)
T: CD56+CD3-IFNγ+
T: CD56+CD3-IFNγ-
S: CD56+CD3-IFNγ+
S: CD56+CD3-IFNγ-
E
X scores (CV acc. = 97%, p < 0.001)
LV2 (Xvar = 17%, Yvar = 0%)
LV1 (Xvar = 45%, Yvar = 40%)
F
VIP Scores
CD8+CD3+IFNγ+
CD8-CD3+IFNγ+
CD56+CD3-IFNγ+
PanCK+MHC I+
CD8-CD3+IFNγ-
CD8+CD3+IFNγ-
CD56+CD3-IFNγ-
PanCK+MHC I-
CD8+CD3+IFNγ+
CD8+CD3+IFNγ-
G
Neighbor score (log10)
H
Tumoral CD8+ T cells
Stromal CD8+ T cells
IFNγ+ (9%)
IFNγ- (91%)
IFNγ+ (1%)
IFNγ- (99%)
MHC I+ PanCK+ Neighbors
T: CD8+CD3+IFNγ+
T: CD8+CD3+IFNγ-
S: CD8+CD3+IFNγ+
S: CD8+CD3+IFNγ-
I
500µm
Merge
CD3
CD8
CD56
IFNγ
MHC I
PanCK
DAPI
100µm
MAD16-101
J
CD56+CD3-IFNg+
panck+ MHC I+ neighbors
panck+ MHC I- neighbors
Summary K Cross Correlation Value
Radius (µm)
CD8+CD3+IFNg+
panck+ MHC I+ neighbors
panck+ MHC I- neighbors
Summary K Cross Correlation Value
Radius (µm)

743

744 **Figure 6. Activated IFNγ+ NK cells and CD8 T cells preferentially associate with other activated**
745 **lymphocytes and MHC-I+ tumor cells.** An OPLSDA model was constructed to discriminate activated and
746 inactivated (IFNγ+/-) NK cells **(A-C)** and CD8 T cells **(E-G)**. A 5-fold cross validation yielded models with
747 96% (NK cells) and 97% (CD8 T cells) classification accuracy. The model outperformed all of 1000 ran-
748 domly permuted models ($p < 0.001$). **(A & E)** The scatter plot shows the X scores on latent variables 1 and
749 2 (LV1 & LV2), where each point represents one cell. **(B & F)** The bar plot shows the Variable Importance
750 in Projection (VIP) scores, artificially oriented in the direction of loadings on LV1 and colored according to
751 their association with activated or inactivated NK cells or CD8 T cells. |VIP score| > 1 indicate a variable
752 with greater than average influence on the projection. **(C & G)** The violin plots show univariate comparisons
753 between top-scoring features. White circles indicate the median. Significance was determined by a two-
754 tailed t-test (* $p < 1x10^{-27}$; ** $p < 1x10^{-30}$; *** $p < 1x10^{-50}$). **(D & H)** Percentage of IFNγ+ NK cells **(D)** and
755 CD8 T cells **(H)** in the tumor and stroma are shown as pie charts. The violin plots show the number of MHC-
756 I+ tumor cell neighbors of IFNγ± lymphocytes in tumor and stroma separately. **(I)** Representative mIF image
757 showing a cluster of activated lymphocytes in an MHC-I-deficient tumor nest. **(J)** The K-cross correlation
758 value is plotted against increasing radii for IFNγ+ NK cells and IFNγ+ CD8 T cells as the target cell and
759 either MHC-I^+ (blue) or MHC-I^- (pink) center cells. 95% confidence intervals are shown in gray, and the
760 black line represents a Poisson (null) distribution.

761